AuNPs Decorated PLA Stereocomplex Micelles for Synergetic Photothermal and Chemotherapy

Xiaoshan Fan[a], Zheng Luo[b], Enyi Ye[*,c], Mingliang You[d], Minting Liu[b], Ye Yun[b], Xian Jun Loh[c], Yun-Long Wu[*,b] , and Zibiao Li[*,c]

[a] State Key Laboratory for Modification of Chemical Fibers and Polymer Materials, Donghua University, Shanghai 201620, China

[b] Fujian Provincial Key Laboratory of Innovative Drug Target Research and State Key Laboratory of Cellular Stress Biology, School of Pharmaceutical Sciences, Xiamen University, Xiamen 361102, China.

[c] Institute of Materials Research and Engineering, A*STAR (Agency for Science, Technology and Research), 2 Fusionopolis Way, Innovis, #08-03, Singapore 138634,
Singapore.

[d] Hangzhou Cancer Institute, Key Laboratory of Clinical Cancer Pharmacology and Toxicology Research of Zhejiang Province, Affiliated Hangzhou Cancer Hospital，Zhejiang University School of Medicine，Hangzhou, 310002 China

Correspondence to yeey@imre.a-star.edu.sg; wuyl@xmu.edu.cn; or lizb@imre.a-star.edu.sg

Abstract

In this work, we design a unique platform for combined photothermal and chemotherapy using PLA stereocomplex (PLA SC) micelles induced hybrid gold nanocarriers. The PLA SC micelles, made from the self-assembly of poly(ethylene glycol)-block-poly(L-lactide) (PEG-PLLA) and poly(2-(dimethylamino) ethyl methacrylate)-block-poly(D-lactide) (PDMAEMA-PDLA, for the first time were used as a template to fabricate the hybrid PLA SC@Au core-shell nanocarriers, in which the anticancer drugs were encapsulated within the core, while the Au nanoparticles were tethered in the shell *via* the *in-situ* reduction of $AuCl_4^-$ by PDMAEMA. The obtained PLA SC@Au hybrid nanocarriers exhibit low toxicity and remarkable photothermal effect. Upon near-infrared (NIR) laser irradiation, the on-site photothermal therapy could further induce an accelerated drug release from the hybrid nanocarrier reservoir via hyperthermia heating of the nanocarriers, thus leading to a synergistic photothermal and chemotherapy towards a significantly improved efficacy in tumor shrinkage. The as-designed PLA SC@Au hybrid nanocarriers, with their biocompatible compositions, dual-drug delivery characteristics and combined photothermal/chemotherapy, show high potential as a novel platform for cancer treatment.

1. Introduction

Although many medical technologies have been greatly improved, cancer is still one of the most troublesome major medical problems, threatening the lives of thousands of healthy people[1, 2]. In addition to traditional surgery, chemotherapy and radiotherapy, there are many new treatment strategies have emerged in the treatment of cancer such as gene therapy, immunotherapy, photothermal therapy and photodynamic therapy etc [3-5]. However, due to the inherent limitations in each method, such as tumor recurrence caused by surgery, tumor resistance caused by chemotherapy, off-target caused by gene therapy etc., monotherapy is often unsatisfactory in tumor treatment. In recent years, the combination of multiple treatment methods has become clinically popular. Compared with single treatment, combining multiple treatment methods can effectively synergize each other's advantages to achieve better tumor treatment effects while reducing side effects[6-19].

In the past few decades, with the development of nanotechnology and material science, nano-platforms capable of synergizing a variety of cancer treatment methods have sprung up like mushrooms. Among the nanomaterials that build these nano-platforms, Au nanoparticles, including Au nanoshell particles, Au nanorods and Au nanocages, are emerging as one of the widely investigated materials[20-25]. Au nanomaterials can strongly absorb near-infrared (NIR) light and produce localized cytotoxic heat upon NIR irradiation. Thus, they can be used as photothermal therapy for cancer treatment. Polymeric micelles as nanoscale vehicles have been extensively studied for drug delivery, which offers remarkable advantages over the free drugs administration, such as higher solubility, longer circulation time in the biological

systems and improved tumor uptake via active or passive mechanisms[26-32]. A novel multifunctional platform for simultaneous photothermal therapy and chemotherapy was developed by incorporating Au nanoparticles into the drug-loaded micelles. Upon NIR irradiation, cytotoxic heat is locally generated due to NIR resonance of Au nanoparticles, and the elevated temperature would accelerate the drug release from the micelles, resulting in the synergetic therapy effect. Thus, a higher therapeutic efficacy has been achieved as the Au nanoparticles conjugated micelles used for cancer treatment. However, the process to construct the Au nanoparticles conjugated micelles is often complicated, limiting their biomedical applications[33-36].

In this present work, we describe a simple yet versatile strategy for the preparation of Au nanoparticles conjugated micelles, as shown in Scheme 1. The stable PLA SC micelles were first prepared through the self-assembly of PEG-PLLA and PDMEMA-PDLA in aqueous solution. The strong stereocomplexation interaction between the PLLA and PDLA segments in the hydrophobic core provided the noncovalent driving force to stabilize the as-formed micelles[37, 38]. Then, the PLA SC micelles were used as templates to fabricate the PLA SC@Au nanoparticles. The shell-forming PDMAMEA served as a reducing agent to reduce Au^{3+} to Au^{0} *via* a one-step *in situ* reduction reaction, and at meanwhile it stabilized the as-formed gold nanoparticles by preventing them from aggregation. Moreover, the PEG can further enhance the stability and biocompatibility of the obtained complex nanoparticles due to its highly hydrated ability. The resulting PLA SC@Au nanoparticles were proven to exhibit light-responsive drug release when being subjected to near-infrared (NIR) irradiation. When combined with NIR irradiation, PLA SC@Au/DOX nanoparticles showed greater

therapeutic efficacy than that of the treatment with PLA SC@DOX, PLA SC@Au or PLA SC@Au/DOX without NIR irradiation. Together with the good biocompatibility, light-triggered drug release and higher therapeutic efficacy, it can be anticipated that the unique PLA SC@Au nanoparticles would be an ideal platform for cancer treatment.

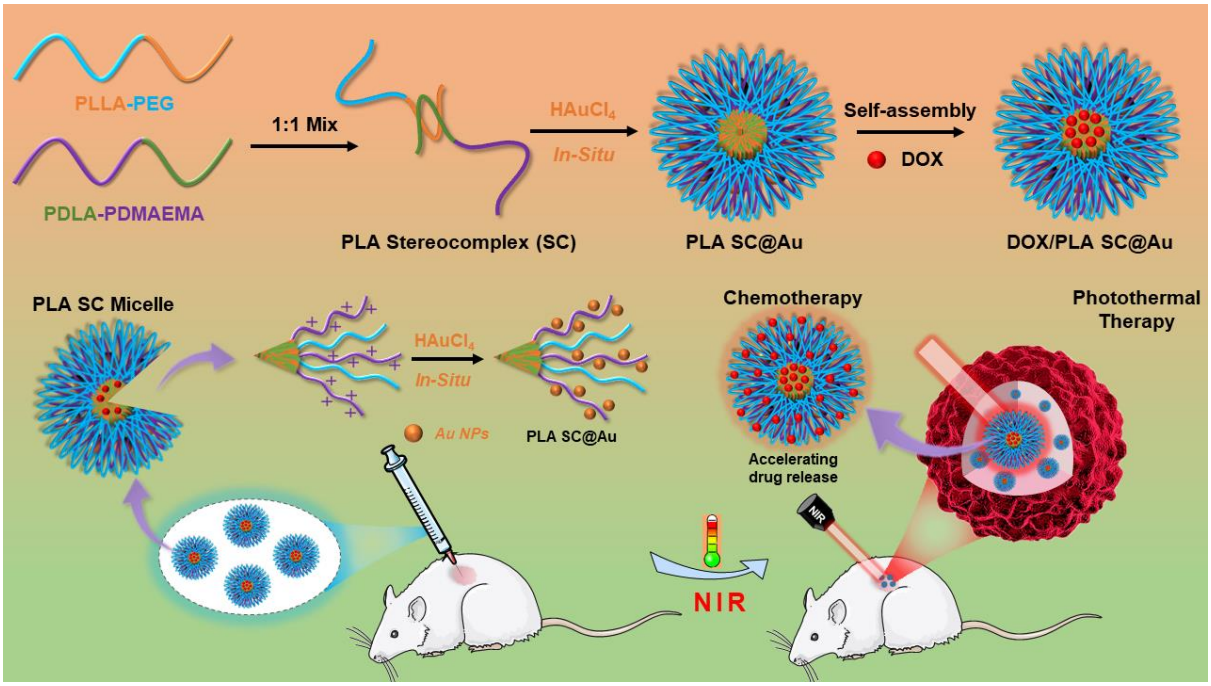

Scheme 1. Schematic representation showing the design strategy of gold nanoparticles decorated PLA SC micelles (PLA SC@Au) for combined photothermal and chemotherapy.

2. Experiments

2.1 Materials

D-Lactide (DLA) and L-lactide (L-LA) monomers were purchased from Purac Biochem and used without further purification. Methoxy poly(ethylene glycol) (mPEG, M_n of 5,000 g/mol), Tin(II) 2-ethylhexanoate ($Sn(Oct)_2$, 95%), toluene (anhydrous, 99.8%), Hydrogen tetrachloroaurate-(III) trihydrate ($HAuCl_4 \cdot 3H_2O$, 99.99%), methanol (anhydrous, 99.8%),

trimethylamine (>99%), 2-bromoisobutyryl bromide (98%), 2-(dimethylamino)ethyl methacrylate (99%), 1,4-dioxane (anhydrous, 99.8%), copper(I) bromide (CuBr, 99%), 1,1,4,7,10,10-hexamethyltriethylenetetramine (HMTETA, 97%), aluminium oxide (neutral), trisodium citrate dihydrate, ethylene glycol (anhydrous, 99.8%), ethanol (>99.8%) and doxorubicin hydrochloride (DOX·HCl) were purchased from Sigma-Aldrich and were used as received. Benzyl alcohol and chloroform were distilled over calcium hydride (CaH_2) before use.

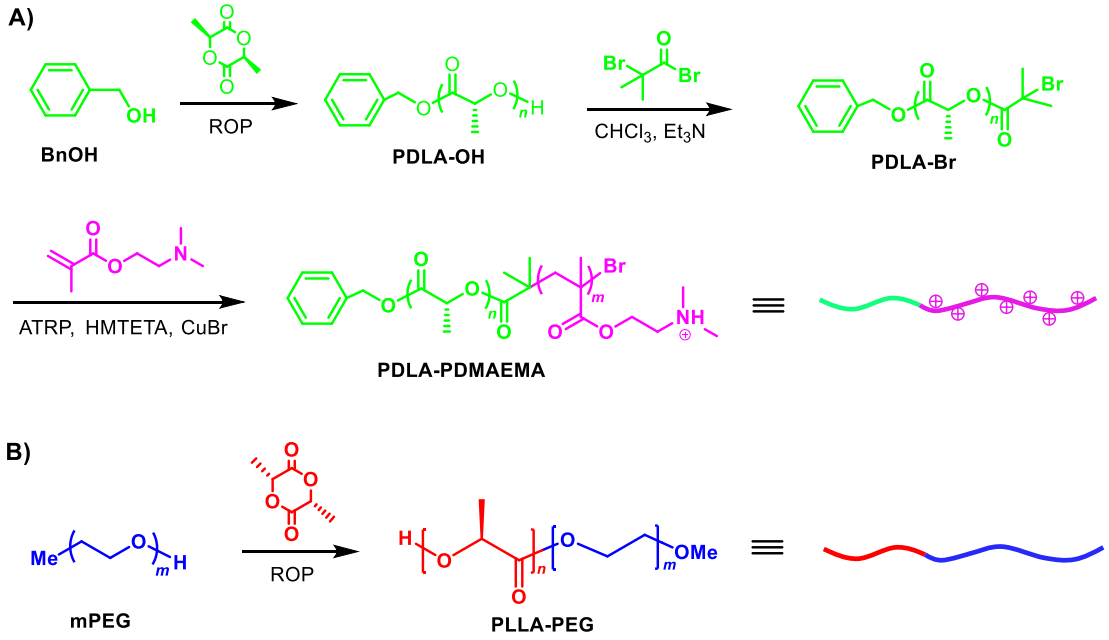

Scheme 2. Synthetic route and schematic illustration of (A) PDMAEMA-PDLA and (B) PEG-PLLA diblock copolymers.

2.2 Synthesis of PDMAEMA-PDLA and mPEG -PLLA diblock copolymers

The block copolymer PDMAEMA-PDLA was synthesized by the combination of ring opening polymerization (ROP) and atom transfer radical polymerization (ATRP) (Scheme 2). Briefly, 15 g of D-lactide monomer, 0.24 mL of benzyl alcohol, and 150 μL of $Sn(Oct)_2$ were

introduced into a 250 mL round-bottom flask in a glovebox. 80 mL of dry toluene was then added to the reactants under nitrogen atmosphere, and the reaction was performed at 130 °C for 24 h under reflux and continuous stirring. Purified product PDLA-OH was obtained by precipitation of the reaction mixture into excess cold methanol twice, followed by overnight vacuum drying at 65 °C (yield, >90%). ($M_{n,NMR}$ = 6,400 g/mol; $M_{n,GPC}$ = 10,310 g/mol, M_w/M_n= 1.20)

The ATRP macroinitiator PDLA-Br was prepared by esterification of its hydroxyl end group with 2-bromoisobutyryl bromide in anhydrous chloroform. A 10 times excess of 2-bromoisobutyryl bromide with respect to OH end groups was added, and triethylamine was used to trap hydrobromic acid generated during the reaction. After six cycles of extractions in trichloromethane/deionized water (1:3, v/v), the reaction mixture was concentrated and precipitated into excess cold methanol twice. PDLA-Br macroinitiator was obtained after drying under vacuum at 50 °C overnight (yield, 92.0%).

For the synthesis of PDMAEMA-PDLA diblock copolymer, 0.5 g of PDLA-Br, 10mL of DMAEMA, and 50 μL of HMTETA were introduced into a 100 mL round-bottom flask containing 9 mL of 1,4-dioxane. Next, the solution was purged and refilled with nitrogen using a vacuum-nitrogen-circling system three times. CuBr was added quickly under nitrogen atmosphere. Polymerization was allowed to proceed under continuous stirring at 75 °C for 24 h. The reaction was stopped by diluting the reaction mixture with THF and exposing it to an ambient atmosphere for 1 h. The catalyst complex was removed by passing the reaction mixture through a short neutral aluminium oxide column. After concentrating the filtrate, the

solution was precipitated into excess hexane and the final products were obtained through centrifugation. ($M_{n,NMR}$ = 26,100 g/mol; $M_{n,GPC}$ = 17,150 g/mol, M_w/M_n= 1.12)

The PEG-PLLA diblock copolymer was prepared by ROP of L-lactide in the presence of monomethoxy PEG (mPEG) and $Sn(Oct)_2$ stannous octoate, according to the reported procedure. (PEG-*b*-PLLA: $M_{n,NMR}$ = 17,540 g/mol; $M_{n,GPC}$ = 25,690 g/mol, M_w/M_n= 1.15)

2.3 Preparation of PLA SC micelles

The stereocomplex micelles were prepared from the mixture of PDMAEMA-PDLA and PEG-PLLA being self-assembly in aqueous solution with equal mass ratio. Briefly, 0.1 g of PEG-PLLA and 0.1 g of PDMAEMA-PDLA copolymers were dissolved in 3mL of anhydrous tetrahydrofuran (THF) and the solution was stirred for 48 h. A 0.5 wt% solution of the stereocomplex micelles was prepared by adding dropwise 0.75 mL of the THF solution into 10 mL of deionized water and exposed to the air to allow the THF to evaporate while stirring for 48 h.

2.4 Preparation of gold nanoparticle conjugates PLA SC@Au

According to the procedure mentioned above, PLA SC solution was first prepared by adding 0.12 g of PEG-PLLA into 5 mL of THF followed by adding the obtained PEG-PLLA solution dropwise into a solution with 0.12 g PDMAEMA-PDLA in 5 mL THF. The obtained solution is stirred for 48 hrs to allow for the PLA SC formation. PLA SC solutions with concentrations ranging from 50 to 600 times of CMC value were prepared by adding pre-determined amount of store solution dropwise into 20 mL of deionized water and

exposed the mixed solutions to air for 48 h to allow the complete THF evaporation.

Taking the mole ratio of DMAEMA and $HAuCl_4$ at 16:1 as a reference, certain amount of $HAuCl_4$ solution was added dropwise into the aqueous solution of PLA SC under vigorous stirring at room temperature in an aluminium foil wrapped flask for 48 h. The obtained red colour PLA SC@Au solution was then dialyzed against deionized water for 24 h to obtain the purified PLA SC@Au nanocarriers (MWCO: 1000 Da).

2.5 Characterization

Gel permeation chromatography (GPC) analysis was done using THF as eluent and monodisperse poly (ethylene glycol) standards were used to obtain the calibration curve. The proton nuclear magnetic resonance (^{1}H NMR) spectra were recorded at 400 MHz and room temperature, the Fourier Transform Infrared spectroscopy (FT-IR), the Dynamic Light Scattering (DLS) with a constant angle of 90^o for measuring hydrodynamic radius was used to characterize structure of polymers and sizes of micelles. Ultraviolet-visible spectroscopy (UV-vis) analysis was done in the range of 300-500 nm at room temperature to determine the critical micelle concentration. Transmission Electron Microscopy (TEM) and DLS measurements were conducted to investigate the size and morphology of the conjugated gold nanoparticles on the produced micelles. Lastly X-Ray Diffraction (XRD) analysis was conducted to verify the self-assembly and formation of stereocomplexes. TEM samples were prepared by dropping micelles solution onto a copper grid covered with carbon followed by drying in a desiccator and were stained by a polymer dye solution that consists of 0.1wt% phosphotungstic acid in 10mL of deionized water. The CMC values of PEG-PLLA,

PDMAEMA-PDLA and PLA SC micelles were determined by using the dye solubilisation method [25]. The CMC measurements were conducted by varying the aqueous polymer concentration in the range of 0.00195 to 0.5wt%, while keeping the concentration and amount of the hydrophobic dye, 1,6-diphenyl-1,3,5-hexatriene (DPH) constant at 0.139 mg/mL. The DPH is prepared by first preparing a store solution of concentration 13.9 mg/mL by dissolving 0.027 g of DPH in 2 mL of THF and adding 0.1mL of the DPH store solution into 9.9 mL of THF. 10 μL of DPH is added to every 1 mL of the polymer solution.

2.6 *In vitro* drug loading and release of DOX loaded micelles

DOX was used as a model drug for *in vitro* drug loading and release. In a typical experiment, 10 mg of PEG-PLLA and PDMAEMA-PDLA were separately dissolved in 1.25 mL of THF and 10 mg of DOX • HCI and 2.5 μL of triethylamine (TEA) were added into the latter solution. After stirred for 24 h, both solutions were mixed together and the combined solution was dialyzed using membrane with a weight cut-off of 1000 in deionized water to remove THF and DOX. After dialysis, aggregates of the unloaded DOX were removed by filtration through a filter with a pore diameter of 0.45μm.

1 mL of DOX loaded SC@Au micelles in dialysis membrane with a molecular weight cut-off of 1000 was submerged in 20 mL of deionised water at 37 ºC in the dark. At predetermined intervals, 1 mL of dialysis solution was collected. The fluorescence intensity of the solutions at 590 nm was measured with an excitation of 440 nm, and the concentration of DOX was determined with reference of a calibration curve.

To measure the drug release from PLA SC@Au mielles with and without NIR irradiation,

two group small flasks containing 5 mL Au micelles/DOX respectively were stirred in dark. At the NIR irradiation group, the samples were irradiated with a NIR laser (808 nm) about 5 min and was stirred for another 30 min before measurement. Based on this method, the samples were irradiated, collected and measured at different time intervals. At the control groups, the samples were just stirred without NIR laser irradiation, then collected and measured at the same time intervals.

2.7 Cell Viability Assay

HepG2 cells were used to evaluate the toxicity of PLA SC@Au by incubating 1×10^4 cells per well in a 96 well plate with differently concentrated samples for 24 h. After that, the medium was replaced by 100 μL fresh medium, and 10 μL MTT solution (5 mg/mL) was added. The cells were incubated for further 4 h, and then 150 μL of DMSO was added to dissolve the resulting purple crystals. The absorbance at wavelength of 490 nm was measured to quantify the cell viability.

2.8 *In vivo* tumor regression study

Three female nude mice with weight of 19 - 21 g were fed in an IVC system and supplied with filtered air, sterile food and water. HepG2 cells were dispersed in sterile phosphate buffered saline (PBS) at a concentration of 1×10^7 cells per milliliter and injected into the flank of nude mice at a volume of 100 μL per mouse. When the solid tumor volume reached around 60 mm^3, mice were divided into 6 groups randomly (each having 3 mice) for receiving different treatment: PBS, PBS and irradiated ($0.5W/cm^2$, 808nm), Au micelles, Au

micelles and irradiated, Au micelles with DOX, Au micelles with DOX and irradiated. Mice weight and tumor volume was measured and calculated every day. After 7 days, the mice were euthanized and tumors were removed for further research. The tissues were then fixed in 15% sucrose solution and 30% sucrose solution orderly for dehydration, and embedded in embedding medium for frozen tissue specimens, cut into 4 μm sections, and stained using hematoxylin and eosin (H&E) for histological analysis. All the experiments were in accordance with the Animal Care Guidelines of Xiamen University.

2.9 Stastical analysis

All charts and data processing were processed using origin 8 analysis software, the experimental data were expressed as mean and variance, and the significance analysis was analyzed using GraphPad 5.0.

3. Results and Discussion

3.1 Synthesis and characterisations of PEG-PLLA and PDMAEMA-PDLA diblock copolymers

According to the designed synthetic routes depicted in Scheme 2, two well-defined amphiphilic block copolymers with narrow molecular weight distribution PEG-PLLA and PDMAEMA-PDLA were successfully synthesized. Due to the stereocomplexation interaction between PLLA and PDLA segments, the mixture of two block copolymers can form stable core-shell micelles in solution, further serving as a template to prepare the unique PLA SC@Au hybrid nanocarriers, in which the inner hydrophobic core can be used drug reservoir

surrounded by the outer shell conjugated with Au nanoparticles. After drug loading, the obtained PLA SC@Au/DOX nanoparticles combine photothermal with chemotherapy together as a new type of stimuli-responsive drug delivery carrier for synergistic therapeutic effect in cancer treatment.

The chemical structures and formations of the products were well characterized by ^{1}H NMR and FT-IR techniques. Figure 1A showed the ^{1}H NMR spectrum of PDLA, in which the characteristic signals (a) and (b) belonging to PDLA can be seen clearly. Compared the ^{1}H NMR spectrum of the ATRP macroinitiator PDLA-Br (Figure 1B) with the precursor PDLA, the new resonance signals at 1.94~1.98 ppm could be assigned to the methyl protons of bromoisobutyryl fragment, indicating the successful transformation of OH end group into bromine. In Figure 1C, the newly appeared signals (d)~(h) were assigned to the characteristic signals of DMAEMA repeated units, conforming the successful synthesis of the block copolymer PDMAEMA-PDLA. The successful synthesis of the block copolymer PEG-PLLA was also confirmed by ^{1}H NMR spectrum (Figure 1D). Additionally, the obtained block copolymers PDMAEMA-PDLA and PEG-PLLA were further characterized by FT-IR spectra (Figure S1). The appearance of typical absorption peaks at 1109 cm^{-1}, 1750 $cm^{-1}$and 2890 cm^{-1}, which are assigned to the PLLA and PEG blocks, respectively, confirmed the successful synthesis of copolymer PEG-PLLA (Figure S1a). In Figure S1b, the absorption peak at 1750 cm^{-1} for C=O bands on PDLA and PDMAEMA segments was observed clearly. Moreover, the other characteristic peaks in PDMAEMA segment were also detected. The absorption bands at 1144 cm^{-1} and 1454 cm^{-1} were ascribed to C−C −N stretching vibration and $-CH_2$ bending vibration, respectively, while absorption bands at 2770 cm^{-1} and 2818 cm^{-1} were

attributed to C−H stretching of the $-N(CH_3)_2$ group and 2942 cm^{-1} for C−H stretching of methyl groups and $-CH_2-$ groups of PDMAEMA.

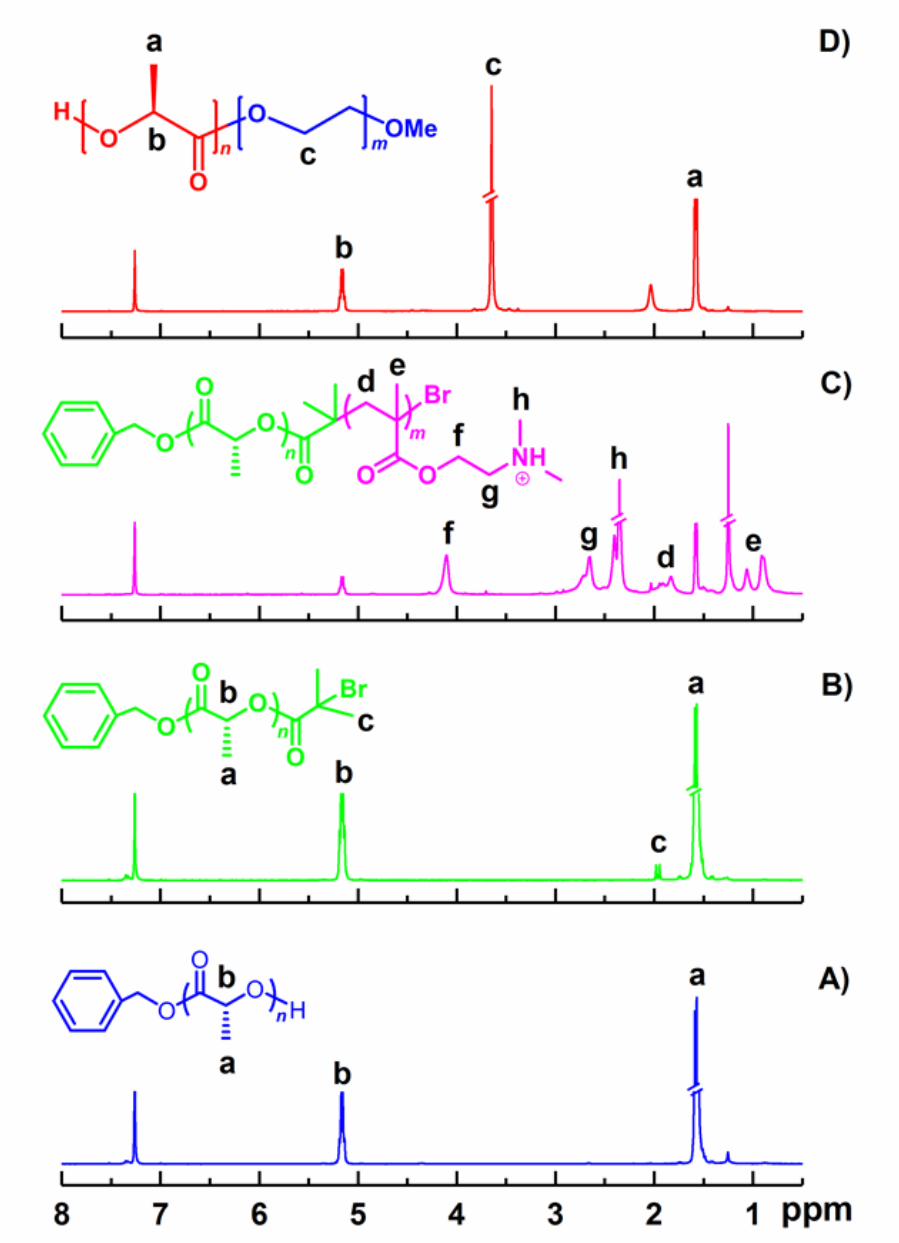

Figure 1. ^1H NMR of (A) PDLA-OH, (B) PDLA-Br, (C) PDMAEMA-PDLA and (D) PEG-PLLA. The peak assignments in (A) and (B) are also applicable to (C).

3.2 PLA SC micelle characteristics

The morphology and size of the micelles will affect the uptake characteristics of any payload encapsulated. In this study, SEM and DLS techniques were used to investigate the morphology and size distribution of the copolymer micelles. From Figure 2A, it can be observed that the TEM image of the as-formed micelles took a spherical morphology with the average diameter about 170 nm. The size of the micelles determined by DLS displayed a unimodal distribution with a narrow polydispersity and an average hydrodynamic diameter about 220 nm. The nano size of the prepared micelles allows them to be less susceptible to uptake by the reticuloendothelial system. It should be noted that the size of the as-formed PLA SC micelles determined by DLS was larger than that recorded by TEM, due to the fact that DLS measured the hydrodynamic size of the micelles, while the drying process for TEM observation caused the shrinkage of the micelles.

The critical micelle concentration (CMC) is one of the most important parameters for assessing the self-assembly process of amphiphilic copolymer and defining the dynamic stability of the formed micelles. Here, the CMC was determined by using fluorescence method with DPH as the probe. Figure 2B showed the changes of the absorbance intensity of DPH with the polymer concentrations, and one can observe that the absorbance of DPH increased with the increase of the polymer concentrations. The CMC value (0.0012 mg/mL) was obtained by extrapolating the absorbance at 378 nm minus the absorbance at 400 nm versus logarithmic concentration.

As the mixture of PEG-PLLA and PDMAEMA-PDLA self-assembled in aqueous solution, the two enantiomers PLLA and PDLA can form stereocomplexes via the interaction between L-lactyl and D-lactyl unit sequences. The resultant stereocomplexation acted as the

noncovalent driving force to enhance kinetic stability of the formed micelles. XRD was employed to confirm the formation of the mixed micelles through the stereocomplexation. As shown in Figure 2C, the mixture of PEG-PLLA and PDMAEMA-PDLA exhibited crystalline peaks at 2θ = 11.9º, 20.8 º and 23.8 º, which corresponded to SC-crystallites as compared with the control sample of the mixture PLLA and PDLA. In addition, we determined the percentage of gold in PLA SC@Au by thermogravimetric analysis to be approximately 3 wt%, and the results are shown in Figure S2. It can be seen from the figure that when the temperature is increased from 100°C to 500°C, the quality of PLA SC@Au has undergone a significant change. We speculate that this is the result of thermal decomposition and oxidative decomposition of the polymer. When the temperature is higher than 700°C, the quality remains basically unchanged, and we infer that the rest should be gold, because gold is relatively stable at this temperature.

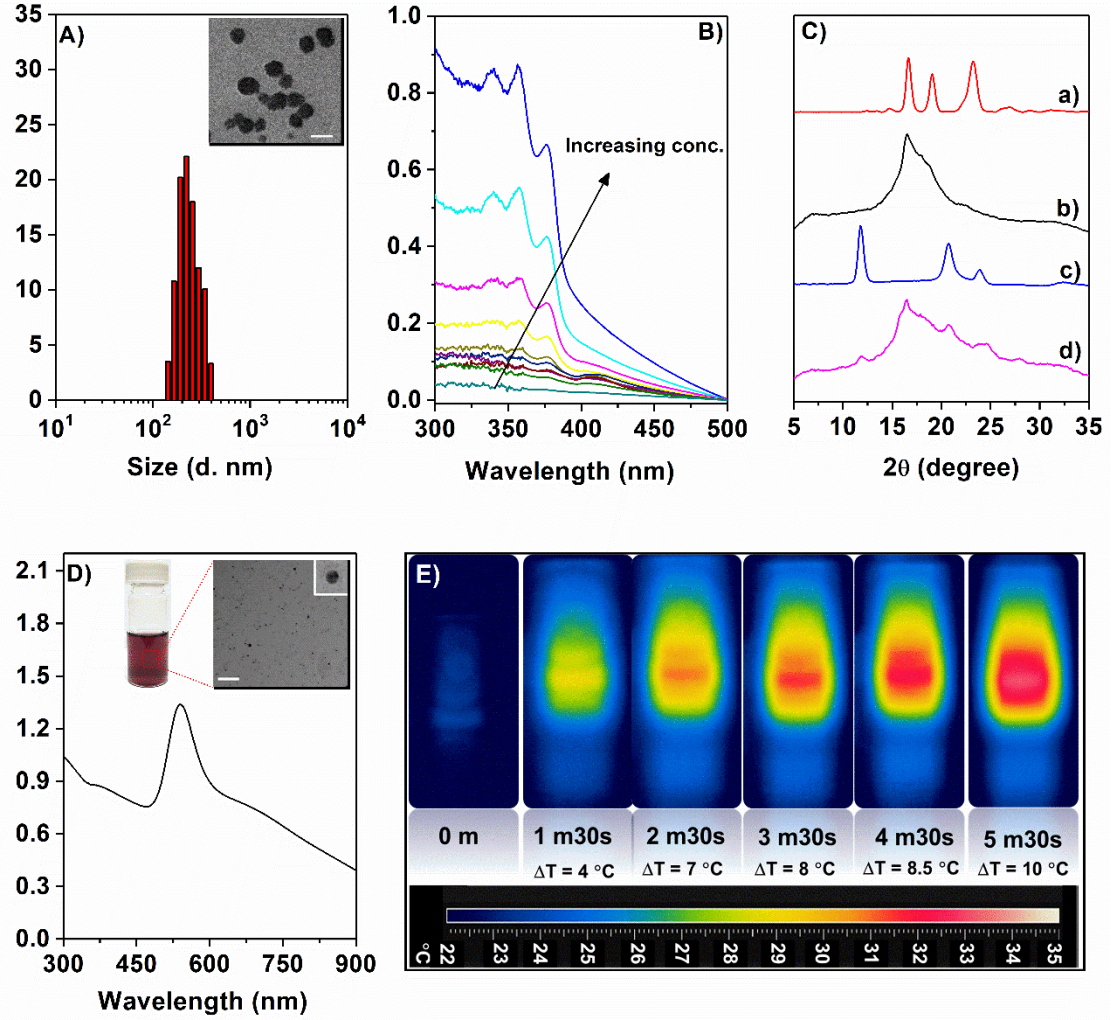

Figure 2. Characterizations of PLA SC and PLA SC@Au nanoparticles. (A) Particle size distribution of PLA SC micelles self-assembled from PEG-PLLA/PDLA-PDMAEMA block copolymers. The inset graphs show the particle morphologies recorded by TEM (scale bar: 200 nm). (B) UV−vis spectra changes of DPH with increasing PLA SC block copolymers concentration from 2.5 × 10^{-3} to 5 mg/mL. (C) XRD spectra of (a) PEG-PLLA, (b) PDLA-PDMAEMA, (c) SC-PLLA/PDLA, (d) SC-PEG-PLLA/PDMAEMA-PDLA. (D) UV−vis spectra of PLA SC@Au nanoparticles. The inset graphs show the as-prepared particle solution and its morphology recorded by TEM (scale bar: 200 nm). (E) Thermal graphic images and temperature increments of PLA SC@Au nanoparticle solution at different laser (808 nm, 1 W/cm^2) irradiation time.

3.3 Gold nanoparticles conjugated PLA SC micelles (PLA SC@Au)

Due to the presence of the shell-forming PDMAEMA and PEG, the PLA SC micelles as-prepared can act as reducing agent to fabricate PLA SC@Au nanoparticles via a coordination–reduction mechanism without additional reductants and stabilizers to further stabilize the Au particles. In the first stage, $AuCl_4^-$ were trapped by the tertiary amine group of PDMAEMA because of the complexation between Au^{3+} and N atom. Then Au^{3+} was self-reduced to zero-valent gold atom at the nucleation stage. Afterward, PLA SC@Au nanoparticles were obtained as the gold atoms combined mutually and grew into GNPs. The UV–vis spectrum of the above PLA SC@Au nanoparticles was shown in Figure 2D, in which the intensive absorption wavelength at 535 nm was caused by the characteristic surface plasmon resonance (SPR) of gold nanoparticles. The TEM image showed that the PLA SC@Au nanoparticles took a nanoscale spherical morphology with the relatively narrow size distribution (Figure 2D). Meanwhile, no nanoparticle aggregation was observed in the TEM image, indicating the PLA SC micelles as stabilizer can effectively stabilize the Au particles.

The PLA SC@Au nanoparticles as-prepared have an absorption peak in the NIR region and heat is locally generated by NIR irradiation. To determine the temperature increase following NIR exposure, the PLA SC@Au nanoparticles solution was exposed to NIR light for 5.5 min using a laser diode ($\lambda \approx 808$ nm), then the temperature of the solution was measured using a thermal imaging camera. After 5.5 min of NIR irradiation, the temperature of the irradiated solution increased by approximately 10 ^{o}C (Figure 2E).

3.4 *In vitro* biological evaluation

In order to verify the drug release ability of PLA SC@Au micelles, we used the anticancer drug DOX as a model molecule to explore the effect of laser irradiation on its drug release behaviour. The cumulative drug release results are shown in Figure 3A. One can see that under NIR irradiation, the drug release rate of DOX-loaded PLA SC@Au micelles is faster, and the cumulative drug release exceeds 90% after 24 h incubation. In the group without laser irradiation, the cumulative drug release was only about 40% in the same period of time. The accelerated drug release under laser irradiation may be caused by the heat generated by the gold nanoparticles which may affect the stability of the micelles by stimulating the chain mobility, thereby creating more channels for drug diffusion. This hybrid nanomaterials, which can accelerate the drug release rate through light stimulation, has the potential for rapid drug release at the tumor site, thereby improving the therapeutic effect of tumor shrinkage.

Cytotoxicity is essential for a good drug carrier. In order to investigate the cytotoxicity of PLA SC@Au, we selected liver cancer cell HepG2 as a cell model, and incubated with PLA SC@Au at different concentrations. As shown in Figure 3B, one can see that the nanocarrier had very low toxicity to HepG2 cells. Even at a concentration of up to 50 μg/ml, more than 60% of the cells can still survive. It can be seen that these PLA SC@Au micelles have good biocompatibility in a broader range of concentration as well as safe potential applications as drug carriers. After that, we explored whether HepG2 cells can effectively take up PLA SC@Au through flow cytometry. From Figure 3C, it can be clearly observed that compared with the control group, the DOX-loaded nanocarriers showed a higher cellular uptake profile. In addition, we also used a live/dead analysis to evaluate the photothermal efficiency in

killing cancer cells. As shown in Figure 3D-E, green fluorescence represents living cells. It can be seen that most of the cells maintained good activity without laser irradiation, and there was more green fluorescence in the field of view. Under laser irradiation, it can be seen that most of the cells in the center zone showed red fluorescence, indicating that most of the cells have lost their vitality (Figure 3E). This is because under laser irradiation, the gold nanoparticles in micelles can convert light into heat energy to effectively ablate tumor cells.

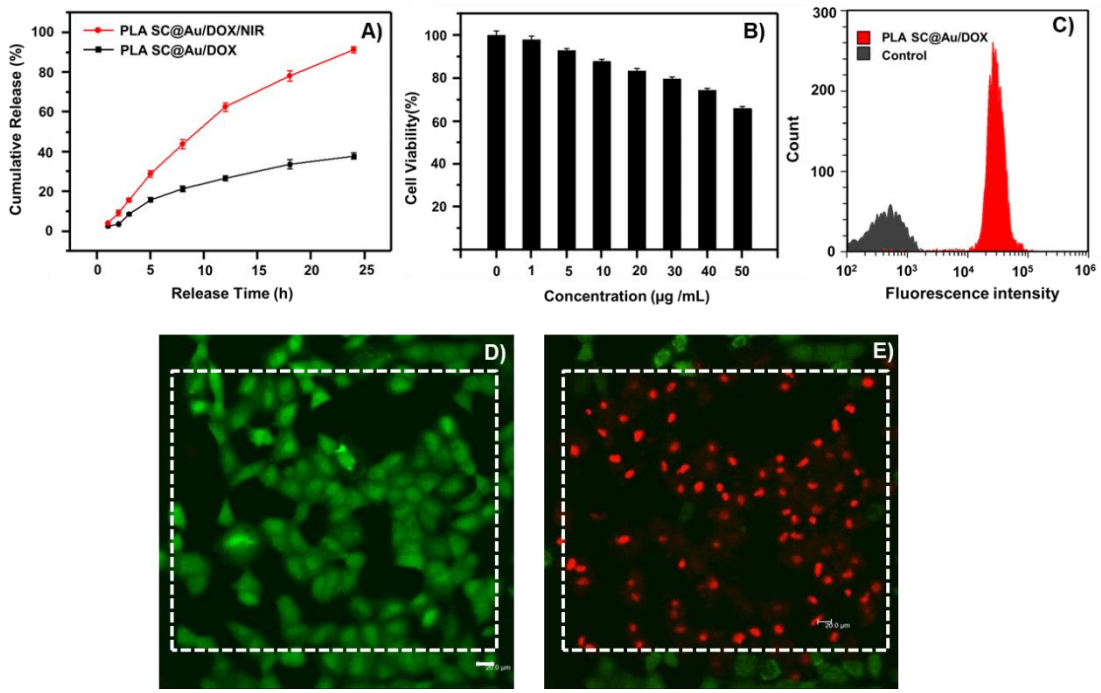

Figure 3. *In vitro* biological evaluation of PLA SC@Au nanoparticles. A) In vitro drug release profiles of DOX-loaded PLA SC@Au nanoparticles with and without NIR irradiation. B) Cell viability assay of HepG2 cells incubated with PLA SC@Au nanoparticles at various concentrations. Data present a mean value with ± standard deviation (SD) (n = 6). C) Flow cytometry analyses of HepG2 cells after incubation with empty (grey) and DOX-loaded PLA SC@Au nanoparticles (red). D-E) In vitro NIR photothermal effect of PLA SC@Au nanoparticles by live/dead assay using confocal fluorescent microscopy images. The living

and dead cells were stained with fluorescein diacetate (green) and propidium iodide (Red), respectively. The Square zones were the area treated with NIR irradiation at 808 nm (1 W/cm^2) (scale bar = 20 μm).

3.5 *In vivo* biological evaluation

In order to verify the therapeutic effect of PLA SC@Au on solid tumors, we inoculated the back of nude mice with HepG2 cells of liver cancer cells to establish a xenograft mouse model for in vivo anti-tumor research. As shown in Figure 4A-B，for both *in vivo* and isolated tumor volume, the treated group showed better tumor growth inhibitory effect than the untreated group. In addition, compared with the single chemotherapy group (PLA SC@Au/DOX) and the photothermal treatment group (PLA SC@Au/NIR), the combined treatment group (PLA SC@Au/DOX/NIR) showed the optimal tumor treatment effect, which may be due to the synergistic effects from photothermal ablation and chemotherapeutic drugs in tumor shrinkage. It is worth noting that the tumor suppression ability of the chemotherapy group alone is significantly lower than that of the photothermal treatment group. In combination with the previous in vitro drug release curve, we speculated that it might be due to the high stability of PLA SC@Au formulation that has limited the rapid release of chemotherapy drugs and thus led to a relatively poor tumor treatment result. From the tumor growth inhibition curve in Figure 4C, it can be seen that after the light-stimulated PLA SC@Au/DOX treatment, the size of the tumor was significantly reduced to 28.4 ± 10.6mm^3, comparing with the tumor size of 648.9 ± 24.4 mm^3 in the control group. In addition, the photothermal therapy group showed a tumor volume similar to that of the combined therapy

group, which shows that photothermal therapy plays a more important role in the combined therapy. In order to explore the toxicity of the nanoformulation to mice, we measured the body weight of the mice for evaluation. It can be seen from Figure 4D that the body weight of the mice in the control group and the treatment group did not show significant changes, which indicates that the nanoformulation is relatively safe and does not affect the body mass of the mice.

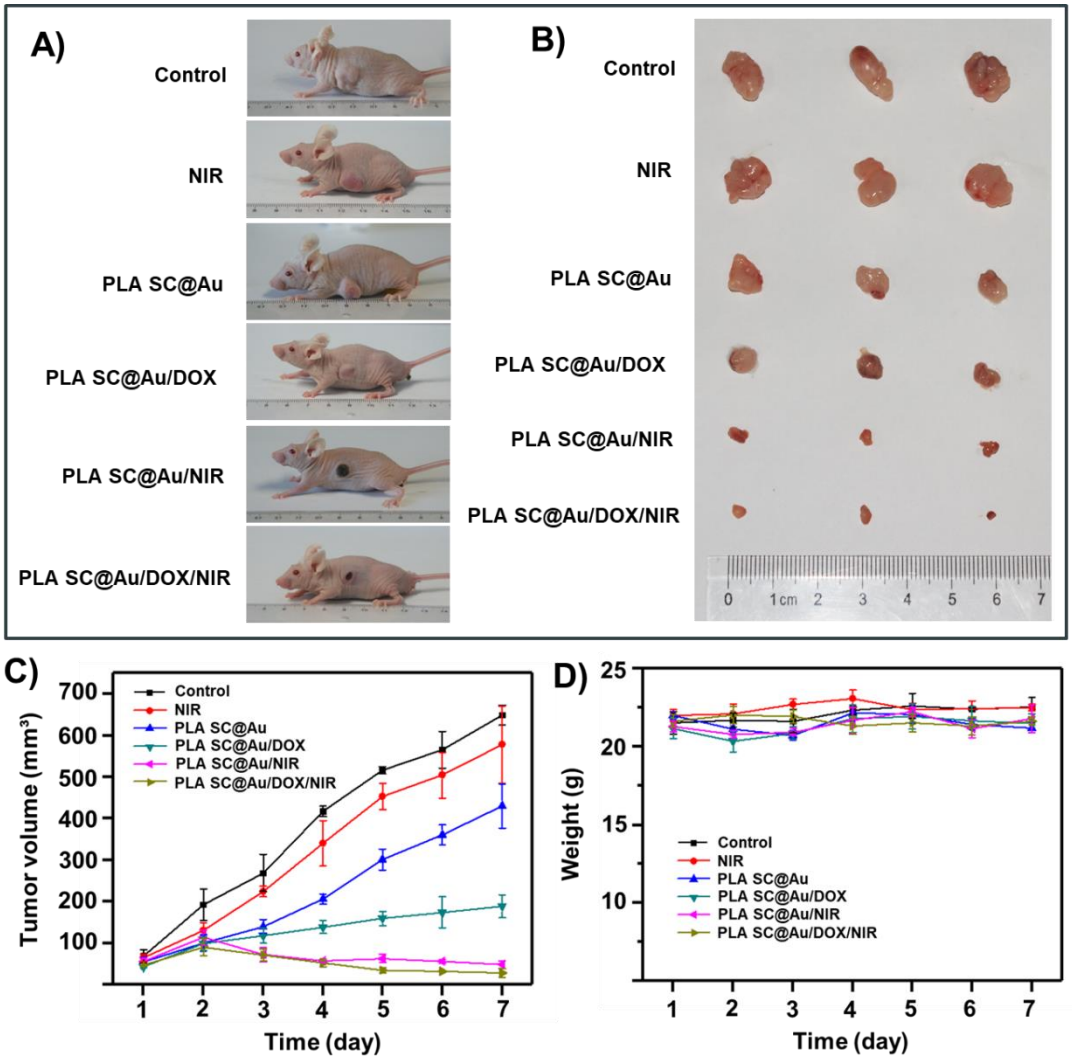

Figure 4. In vivo evaluation of PLA SC@Au nanoparticles for synergetic photothermal and chemotherapy in cancer treatment. A) Photographs of subcutaneous tumors and B) typical

images of excised tumor after treatment by PLA SC@Au nanoparticles under different conditions. C) Tumor growth and D) weight change curves after different treatments for 7 days. The experiments were carried out by 3 mice for each group and results were represented as mean ± SD (n = 3).

3.6 Histopathological analysis

In order to further verify the synergistic anti-tumor effect of PLA SC@Au/DOX combined with photothermal and chemotherapy, we performed frozen sections of the isolated tumors and analyzed the tissue sections with H&E staining. The results of HE staining of tissue sections are shown in Figure 5. Dark purple represents the nucleus, and pink represents the cytoplasm and extracellular matrix. It can be seen from the figure that the tumor tissue sections of the control group, the single laser irradiation group (NIR Only) and the material group (PLA SC@Au) showed a relatively complete cell distribution morphology. Compared with them, those of the treatment group showed fewer tumor cells and larger area of cell apoptosis and loss, in which the combination chemotherapy and photothermal therapy group (PLA SC@AU/DOX/NIR) showed the largest number of cell apoptosis and loss, which may be due to the synergistic effect of the combination therapy leading to better tumor treatment effect. Notably, the photothermal therapy group (PLA SC@AU/NIR) showed more tumor cell apoptosis than the chemotherapy group (PLA SC@Au/DOX), indicating that photothermal therapy dominated the tumor killing effect.

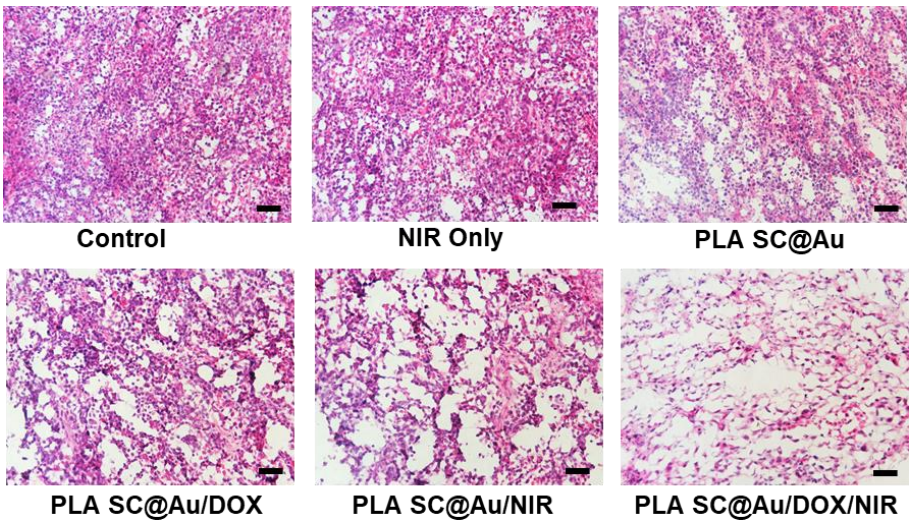

Figure 5. Hematoxylin and eosin staining for the tumor tissues harvested from the mice after different treatments for 7 days (scale bar = 50 μm).

4. Conclusion

In summary, we report a simple yet versatile strategy for the fabrication of a unique drug delivery system combining photothermal therapy and chemotherapy. Two deliberately designed block copolymers, PEG-PLLA and PDMAEMA-PDLA, were utilized to prepare the PLA SC micelles and were further loaded with DOX and Au nanoparticles to produce a novel multifunctional platform PLA SC@Au/DOX for simultaneous photothermal therapy and chemotherapy. The light-responsive drug release capability and therapeutic efficacy of the developed hybrid nanocarriers were systematically investigated. The results revealed that the as-formed multifunctional nanoparticles could deliver encapsulated DOX drugs and heat to the targeted tumor tissue, resulting in complete tumor destruction with NIR irradiation. As compared, the anticancer effectiveness of the chemophotothermal treatment was clearly superior to that of chemotherapy or photothermal therapy alone. Taken together, these results demonstrate that the PLA SC@Au exhibited excellent synergistic effects of

chemophotothermal treatments, providing a simple and practical strategy for combining different cancer treatments.

Acknowledgements

This work is supported by the National Key R&D Program of China (Grant No. 2020YFA0908100), the Natural Science Foundation of China (81773661), and Agency for Science, Technology and Research (A*STAR).

5. References

1. R. L. Siegel, K. D. Miller and A. Jemal, *Ca-a Cancer Journal for Clinicians*, 2019, **69**, 7-34.

2. L. A. Emens, *Clinical Cancer Research*, 2018, **24**, 511-520.

3 D. Li, D. Hu, H. Xu, H. K. Patra, X. Liu, Z. Zhou, J. Tang, N. Slater and Y. Shen, *Biomaterials*, 2021, **264**, 120365.

4. C. Xing, S. Chen, M. Qiu, X. Liang, Q. Liu, Q. Zou, Z. Li, Z. Xie, D. Wang, B. Dong, L. Liu, D. Fan and H. Zhang, *Advanced Healthcare Materials*, 2018, **7**, 1701510.

5. W. Tao, N. Kong, X. Ji, Y. Zhang, A. Sharma, J. Ouyang, B. Qi, J. Wang, N. Xie, C. Kang, H. Zhang, O. C. Farokhzad and J. S. Kim, *Chemical Society Reviews*, 2019, **48**, 2891-2912.

6. J.-Y. Zeng, M.-K. Zhang, M.-Y. Peng, D. Gong and X.-Z. Zhang, *Advanced Functional Materials*, 2018, **28**, 1705451.

7. L. Shao, R. Zhang, J. Lu, C. Zhao, X. Deng and Y. Wu, *Acs Applied Materials & Interfaces*, 2017, **9**, 1226-1236.

8. Y. Jiang, D. Cui, Y. Fang, X. Zhen, P. K. Upputuri, M. Pramanik, D. Ding and K. Pu, *Biomaterials*, 2017, **145**, 168-177.

9. X. Liang, X. Ye, C. Wang, C. Xing, Q. Miao, Z. Xie, X. Chen, X. Zhang, H. Zhang and L. Mei, *Journal Of Controlled Release*, 2019, **296**, 150-161.

10. Q. Chen, L. Xu, C. Liang, C. Wang, R. Peng and Z. Liu, *Nature Communications*, 2016, **7**,1-13.

11. J. Li, D. Cui, J. Huang, S. He, Z. Yang, Y. Zhang, Y. Luo and K. Pu, *Angewandte Chemie-International Edition*, 2019, **58**, 12680-12687.

12. J. Nam, S. Son, K. S. Park, W. Zou, L. D. Shea and J. J. Moon, *Nature Reviews Materials*, 2019, **4**, 398-414.

13. X. Duan, C. Chan, N. Guo, W. Han, R. R. Weichselbaum and W. Lin, *Journal Of the American Chemical Society*, 2016, **138**, 16686-16695.

14. J. Feng, Z. Xu, F. Liu, Y. Zhao, W. Yu, M. Pan, F. Wang and X. Liu, *Acs Nano*, 2018, **12**, 12888-12901.

15. Y. Chang, Y. Feng, Y. Cheng, R. Zheng, X. Wu, H. Jian, D. Zhang, Z. Tang, Z. Wang, J. Hao and H. Zhang, *Advanced Science*, 2019, **6**, 1900158.

16. S. M. Ayuk and H. Abrahamse, *Cells*, 2019, **8**, 431.

17. Q. Huang, S. Zhang, H. Zhang, Y. Han, H. Liu, F. Ren, Q. Sun, Z. Li and M. Gao, *Acs Nano*, 2019, **13**, 1342-1353.

18. Y. Duo, Y. Huang, W. Liang, R. Yuan, Y. Li, T. Chen and H. Zhang, *Advanced Functional Materials*, 2020, **30**, 1906010.

19. Z. Guo, S. Zhu, Y. Yong, X. Zhang, X. Dong, J. Du, J. Xie, Q. Wang, Z. Gu and Y. Zhao, *Advanced Materials*, 2017, **29**, 1704136.

20. F. Farjadian, A. Ghasemi, O. Gohari, A. Roointan, M. Karimi and M. R. Hamblin, *Nanomedicine*, 2019, **14**, 93-126.

21. T. D. Brown, N. Habibi, D. Wu, J. Lahann and S. Mitragotri, *Acs Biomaterials Science & Engineering*, 2020, **6**, 4916-4928.

22. X. Sun, X. Huang, X. Yan, Y. Wang, J. Guo, O. Jacobson, D. Liu, L. P. Szajek, W. Zhu, G. Niu, D. O. Kiesewetter, S. Sun and X. Chen, *Acs Nano*, 2014, **8**, 8438-8446.

23. F. Silva, A. Zambre, M. P. C. Campello, L. Gano, I. Santos, A. M. Ferraria, M. J. Ferreira, A. Singh, A. Upendran, A. Paulo and R. Kannan, *Bioconjugate Chemistry*, 2016, **27**,

1153-1164.

24. B. Pang, Y. Zhao, H. Luehmann, X. Yang, L. Detering, M. You, C. Zhang, L. Zhang, Z.-Y. Li, Q. Ren, Y. Liu and Y. Xia, *Acs Nano*, 2016, **10**, 3121-3131.

25. S. Yook, Y. Lu, J. J. Jeong, Z. Cai, L. Tong, R. Alwarda, J.-P. Pignol, M. A. Winnik and R. M. Reilly, *Biomacromolecules*, 2016, **17**, 1292-1302.

26. J. Porter, Y. Ding, S. J. M. Hale, R. D. Perrins, A. Robinson, M. P. Mazanetz, Y. Wu, Y. Ma, K. Conlon and T. Coulter, *Bioorganic & Medicinal Chemistry Letters*, 2020, **30**, 127634.

27. J. Liao, H. Peng, C. Liu, D. Li, Y. Yin, B. Lu, H. Zheng and Q. Wang, *Materials science & engineering. C, Materials for biological applications*, 2021, **118**, 111527-111527.

28. T. Lang, Z. Zheng, X. Huang, Y. Liu, Y. Zhai, P. Zhang, Y. Li and Q. Yin, *Advanced Functional Materials*, 2020, **2007402**, 1-12.

29. Z. Yu, H. Li, Y. Jia, Y. Qiao, C. Wang, Q. Zhou, X. He, S. Yu, T. Yang and H. Wu, *Polymer Chemistry*, 2020, **11**, 7330-7339.

30. X. Fan, H. Cheng, X. Wang, E. Ye, X. J. Loh, Y.-L. Wu and Z. Li, *Advanced Healthcare Materials*, 2018, **7**, 1701143.

31. Y. Liu, C. Xu, X. Fan, X. J. Loh, Y.-L. Wu and Z. Li, *Materials Science & Engineering C-Materials for Biological Applications*, 2020, **108**, 110464.

32. X. Fan, J. Yang, X. J. Loh and Z. Li, *Macromolecular Rapid Communications*, 2019, **40**, 1800203.

33. H. Moustaoui, D. Movia, N. Dupont, N. Bouchemal, S. Casale, N. Djaker, P. Savarin, A. Prina-Mello, M. L. de la Chapelle and J. Spadavecchia, *Acs Applied Materials & Interfaces*, 2016, **8**, 19946-19957.

34. S.-M. Lee, H. Park, J.-W. Choi, Y. N. Park, C.-O. Yun and K.-H. Yoo, *Angewandte Chemie-International Edition*, 2011, **50**, 7581-7586.

35. T. Cui, J.-J. Liang, H. Chen, D.-D. Geng, L. Jiao, J.-Y. Yang, H. Qian, C. Zhang and Y. Ding, *Acs Applied Materials & Interfaces*, 2017, **9**, 8569-8580.

36. S.-M. Lee, H. J. Kim, Y.-J. Ha, Y. N. Park, S.-K. Lee, Y.-B. Park and K.-H. Yoo, *Acs Nano*, 2013, **7**, 50-57.

37. W. Li, X. Fan, X. Wang, X. Shang, Q. Wang, J. Lin, Z. Hu and Z. Li, *Materials Science*

& Engineering C-Materials for Biological Applications, 2018, **91**, 688-695.

38. Z. Li, D. Yuan, G. Jin, B. H. Tan and C. He, *Acs Applied Materials & Interfaces*, 2016, **8**, 1842-1853.

Supporting information

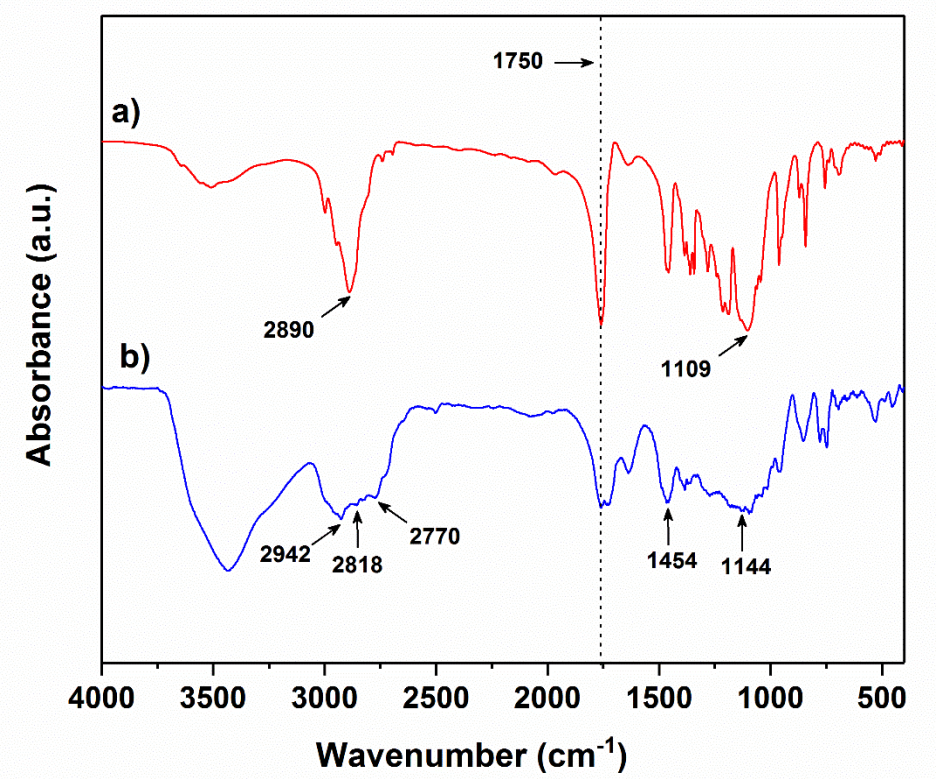

Figure S1. FT-IR spectra of (a) PLLA-PEG and (b) PDLA-PDMAEMA diblock copolymers.

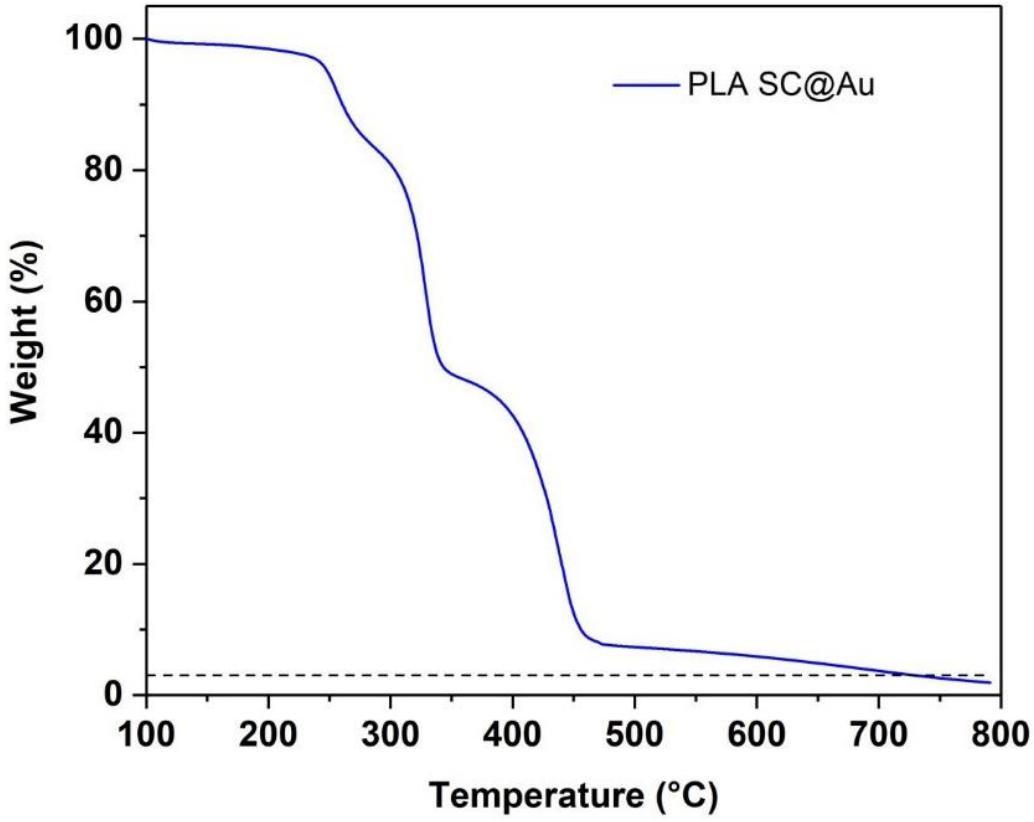

Figure S2. Thermal gravimetric analysis of PLA SC@Au.